Environ. Res. Lett. **7** (2012) 014005 (9pp) doi:10.1088/1748-9326/7/1/014005

Atmospheric stability affects wind turbine power collection

Sonia Wharton[1] **and Julie K Lundquist**[2,3]

[1] Atmospheric, Earth and Energy Division, Lawrence Livermore National Lab, PO Box 808, L-103, Livermore, CA 94551, USA
[2] Department of Atmospheric and Ocean Sciences, University of Colorado at Boulder, CUB-311, Boulder, CO 80309, USA
[3] National Renewable Energy Laboratory, Golden, CO 80401, USA

Received 19 September 2011
Accepted for publication 14 December 2011
Published 12 January 2012
Online at stacks.iop.org/ERL/7/014005

Abstract
The power generated by a wind turbine largely depends on the wind speed. During time periods with identical hub-height wind speeds but different shapes to the wind profile, a turbine will produce different amounts of power. This variability may be induced by atmospheric stability, which affects profiles of mean wind speed, direction and turbulence across the rotor disk. Our letter examines turbine power generation data, segregated by atmospheric stability, in order to investigate power performance dependences at a West Coast North American wind farm. The dependence of power on stability is clear, regardless of whether time periods are segregated by three-dimensional turbulence, turbulence intensity or wind shear. The power generated at a given wind speed is higher under stable conditions and lower under strongly convective conditions: average power output differences approach 15%. Wind energy resource assessment and day ahead power forecasting could benefit from increased accuracy if atmospheric stability impacts were measured and appropriately incorporated in power forecasts, e.g., through the generation of power curves based on a range of turbulence regimes.

Keywords: wind turbines, wind power, atmospheric stability, wind shear, turbulence

1. Introduction

While the average wind speed in a turbine rotor disk largely determines the amount of power that is generated, wind shear and turbulence intensity also influence power output (e.g., Motta *et al* 2005, Sumner and Masson 2006, Gottschall and Peinke 2008, van den Berg 2008). A dependence of power performance on atmospheric stability has been observed previously (Christensen and Dragt 1986, Fransden 1987, Elliott and Cadogan 1990, Rohatgi and Barbezier 1999), although few of these studies have analyzed power output from modern turbines with hub heights above 60 m. More recently, studies have focused on the sensitivity of power curves to stability-related characteristics including wind shear (Rareshide *et al* 2009, Wagner *et al* 2009) and turbulence intensity (Kaiser *et al* 2003, Honhoff 2007, Tindal *et al* 2008).

Conclusions vary dramatically on the effects of stability on power generation. At a US Great Plains wind farm, Rareshide *et al* (2009) found that moderate to high positive wind shear led to higher power output than when wind shear was low. In contrast, a modeling study by Wagner *et al* (2009), based on turbines on flat Danish terrain, suggested that very high positive wind shear decreased power by 26%, as compared to no shear conditions. As stability also is related to atmospheric turbulence, others have suggested that separate power curves for different turbulent conditions be calculated to distinguish the effects of turbulence on power production (Elliott and Cadogan 1990). This may be especially important for downwind turbines within wind farms, as chaotic and turbulent wake flows increase stress on downstream turbines (Mann *et al* 2008). Despite such studies, power curves are usually presented as a function of hub-height wind speed alone, without information on wind velocity and turbulence intensity across the rotor disk (IEC 2003).

In our study, we quantify the influence of atmospheric stability on power performance using wind profile data from a

3-axis sonic detection and ranging (SODAR), investigating a full range of stability parameters including turbulence kinetic energy (TKE), vertical turbulence intensity (I_w), horizontal turbulence intensity (I_U), and the wind shear coefficient (α). The stability parameters are described in detail in (Wharton and Lundquist 2012). This present study is the first letter to our knowledge to explore the relationship between three-dimensional turbulence and turbine power production.

2. Data and methods

2.1. Wind farm overview

Power data from July 2007 to June 2008 were collected at a multi-MW wind farm in western North America at an elevation near sea level. Strong land–ocean temperature differences, particularly during the summer, drive strong local southwesterly winds. The landscape is grass-covered rolling hills, with subtle elevation changes. In addition to turbine power data, meteorological data from an 80 m tall tower, SODAR and turbine-mounted cup anemometers were also used. A map of the wind farm and instrument locations is found in (Wharton and Lundquist 2012).

A subset of 80 m tall, horizontal-axis, three-bladed wind turbines, with rotor diameters of approximately 80 m, was selected for analysis. The turbines are pitch controlled. The exact type and make of the turbines is not disclosed here for proprietary reasons. The turbines were selected to ensure that they did not experience wakes from other turbines or upwind hills, i.e., the distance between an upwind obstacle and downwind turbine was verified to ensure that the turbine was no closer than four rotor diameters (IEC 2003). The turbines generated power based on the wind between 40 and 120 m above ground level (AGL). Hub-height (80 m) wind speed was measured with cup anemometers (NRG IceFree, NRG Systems, Hinesburg, VT, USA) located downwind of each turbine's nacelle hub.

The meteorological tower was equipped with cup anemometers at 50, 60 and 80 m AGL to measure wind speed at a sampling rate of 1 Hz and accuracy of 0.3 m s^{-1}. High resolution vertical profiles of wind speed, direction, and three-dimensional turbulence were available from a three beam, 4500 Hz Doppler mini SODAR (Model4000, Atmospheric Systems Corporation, Santa Clarita, CA, USA). The SODAR measured 3-axis wind speeds (u, v and w), with a sampling rate of 1 Hz per beam and a vertical resolution of 10 m, from 20 to 200 m AGL. The data were quality controlled according to accepted SODAR standards (e.g. Antoniou *et al* 2003) (see Wharton and Lundquist 2012).

2.2. Assessment of atmospheric stability

A dimensionless wind shear exponent (α) was calculated from wind speed at two heights 1 and 2 using the simple power law (Elliott *et al* 1987):

$$U_2(z) = U_1\left(\frac{z_2}{z_1}\right)^{\alpha} \tag{1}$$

where U is mean horizontal wind speed (m s^{-1}) at height z (m). The wind shear exponent approximates atmospheric stability but it is not a direct measure of stability. Separate wind shear exponents were calculated across heights of 50 and 80 m at the meteorological tower and from the SODAR at heights of 40 and 80 m (bottom half of a turbine rotor disk), 80 and 120 m (top half), and 40 and 120 m (entire disk).

Turbulence intensity (I_U, %) includes direct measurements of horizontal turbulence fluctuations in the wind field. Turbulence intensity was calculated from a cup anemometer:

$$I_{U\_\mathrm{cup}} = \frac{\sigma_U}{U} \tag{2}$$

where U is mean horizontal wind speed (m s^{-1}) at 80 m and σ_U is standard deviation (m s^{-1}) of U at 80 m over a 10 min averaging period. SODAR estimates of turbulence intensity also were calculated:

$$I_{U\_\mathrm{SODAR}} = \frac{\sqrt{(\sigma_u^2 + \sigma_v^2)}}{U} \tag{3}$$

where σ_u^2 is variance in latitudinal wind speed (u, m s^{-1}) and σ_v^2 is variance in longitudinal wind speed (v, m s^{-1}). In both equations, higher I_U magnitudes indicate more turbulence in the wind field. Note that I_{U_cup} and I_{U_SODAR} are different quantities, as discussed in Wharton and Lundquist (2012).

Some investigators have reported tendencies for SODARs to overestimate horizontal velocity variances (e.g., Gaynor and Kristensen 1986, Ito 1997) which would lead to higher turbulence estimates; however, these errors are not included in the vertical velocity component. Therefore, a SODAR vertical turbulence intensity (I_W, %) was calculated based on standard deviations in the vertical velocity (σ_w) at 80 m:

$$I_w = \frac{\sigma_w}{U}. \tag{4}$$

Lastly, related to turbulence intensity, turbulence kinetic energy (TKE, m^2 s^{-2}) was calculated from the SODAR:

$$\mathrm{TKE} = \tfrac{1}{2}(\sigma_u^2 + \sigma_v^2 + \sigma_w^2) \tag{5}$$

where σ_u^2, σ_v^2, and σ_w^2 are variance in latitudinal (u), longitudinal (v), and vertical (w) velocities (m s^{-1}) at 80 m. TKE is a direct measure of the intensity of three-dimensional turbulence.

In prior work, we documented confidence in the SODAR stability parameters via a comparison with a robust measurement of stability, the Obukhov length (L) and classified each 10 min period as belonging to one of five stability classes: strongly stable, stable, near-neutral (includes slightly stable, neutral, and slightly convective), convective, or strongly convective (see Wharton and Lundquist 2012). Thresholds for each stability class and descriptions of related boundary layer conditions are listed in table 1.

2.3. Evaluation of power performance

Power curves (turbine power output versus wind speed) were calculated using 10 min averages of power (kW) from each of the six turbines. Manufacturer's ('expected') power curves

Table 1. Thresholds for wind shear and turbulence during the five major stability classes, as well as associated boundary layer properties.

Stability class	Boundary layer properties	Hub-height wind speed	Wind shear	Turbulence
Strongly stable	Highest shear in swept-area, nocturnal LLJ may be present, little turbulence except just below the LLJ	Strong, especially at night	Highest: $\alpha > 0.3$	Lowest: $I_U < 8\%$; $I_w < 4\%$; TKE < 0.4 m^2 s^{-2}
Stable	High wind shear in swept-area, low amount of turbulence unless a nocturnal LLJ is present	Strong, especially at night	High: $0.2 < \alpha < 0.3$	Low: $8\% < I_U < 10\%$; $4\% < I_w < 6\%$; $0.4 <$ TKE < 0.7 m^2 s^{-2}
Near-neutral	Logarithmic wind profile	Generally strongest	Moderate: $0.1 < \alpha < 0.2$	Moderate: $10\% < I_U < 13\%$; $6\% < I_w < 9\%$ $0.7 <$ TKE < 1.0 m^2 s^{-2}
Convective	Lower wind speeds, low shear in swept-area, high amount of turbulence	Low	Low: $0.0 < \alpha < 0.1$	High: $13\% < I_U < 20\%$; $9\% < I_w < 17\%$ $1.0 <$ TKE < 1.4 m^2 s^{-2}.
Strongly convective	Lowest wind speeds, very little wind shear in swept-area, highly turbulent	Lowest	Lowest: $\alpha < 0.0$	Highest: $I_U > 20\%$; $I_w > 17\%$; TKE > 1.4 m^2 s^{-2}.

provided comparisons to the wind farm observations. The amount of power theoretically available to a turbine, at time i, is expressed as the energy flux (P_i, Watts):

$$P_i = 0.5\rho_a A_t U_i^3 \tag{6}$$

where ρ_a is air density (kg m^{-3}), A_t is area of a turbine rotor disk (m^2), and U_i is instantaneous wind speed (m s^{-1}). However, the extraction of power from the wind is not 100% efficient and the theoretical, maximum mechanical efficiency of a turbine is just 59.3% (Betz 1966).

In our study, power performance by an individual turbine was evaluated using normalized power (P_{norm}, %):

$$P_{\text{norm}}(t, i) = \frac{P_{t,i}}{P_{\text{rated}}} \times 100 \tag{7}$$

where $P_{t,i}$ is the average amount of power (kW) generated at turbine t over a 10 min time period i and P_{rated} is the maximum amount of power (kW) that turbine t is potentially able to produce, as determined by the manufacturer. A P_{norm} of 100% indicates that a turbine produced power equal to the manufacturer's maximum rating. P_{norm} was calculated for each of the six turbines for every 10 min period.

2.4. Calculation of equivalent wind speed

Hub-height wind speed may not represent the flow across the entire rotor disk. Recent work by Wagner *et al* (2009) and Antoniou *et al* (2007) suggest calculating a speed representative of the disk area for use in power curves. Following Sumner and Masson (2006), 10 min average SODAR data, at nine measurement heights from 40 to 120 m, were used to calculate a rotor-averaged or equivalent wind speed ($U_{\text{equiv\_SODAR}}$, m s^{-1}) across heights representing the rotor disk:

$$U_{\text{equiv\_SODAR}} = \frac{2}{A_t} \int_{H-r}^{H+r} U(z)(r^2 - H^2 + 2Hz - z^2)^{1/2}\,\mathrm{d}z \tag{8}$$

where $U(z)$ is mean wind speed (m s^{-1}) at height z (m), r is radius of the rotor disk (m), H is hub-height (m), z is measurement height (m), and dz is 10 m. This integral over the rotor disk altitudes was evaluated via summation using the SODAR data at discrete 10 m vertical intervals. Only vertical variability is measured and included in this interval as horizontal homogeneity is assumed.

Further, following Wagner *et al* (2009), equation (8) was modified to recognize that the instantaneous wind speed is a composite of both mean (U) and turbulent (σ_U) components. To incorporate any turbulent energy encountered by the rotor, a modified 'true-flux' equivalent wind speed ($U_{\text{equivTI\_SODAR}}$, m s^{-1}) was calculated:

$$U_{\text{equivTI\_SODAR}} = \frac{2}{A_t} \int_{H-r}^{H+r} U_I(z)(r^2 - H^2 + 2Hz - z^2)^{1/2}\,\mathrm{d}z \tag{9}$$

where wind speed at each height $U_I(z)$ has now been 'corrected' to include any additional energy from turbulence:

$$U_I(z) = \sqrt[3]{U^3(z)(1 + 3I_U^2)}. \tag{10}$$

Note that equation (9) assumes that the wind turbine is able to extract energy from turbulent motions in the air stream.

The SODAR was located between 3 and 4.8 km from the turbines discussed, making it difficult to justify directly using the SODAR 'true-flux' equivalent wind speed in the

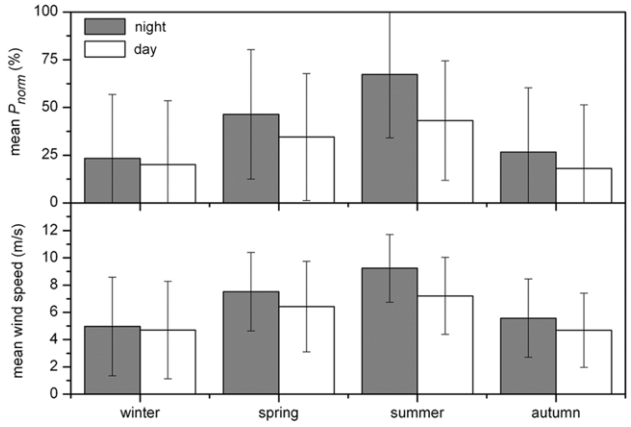

Figure 1. Mean seasonal (± one standard deviation) normalized power (P_{norm}) and nacelle (80 m) wind speed for all six turbines during nighttime and daytime hours. This site experiences strongest hub-height wind speeds and power production during summer nights while wind speed and power production are minimal during autumn and winter months.

power curves. To adjust for any localized differences in wind speed between SODAR and turbines, we first assumed that differences between SODAR hub-height wind speed U_{80_SODAR} and SODAR 'true-flux' equivalent wind speed $U_{\text{equivTI\_SODAR}}$ could be considered a constant (over a 10 min period) across the wind farm. Next, the turbine nacelle (80 m) wind speed U_{nacelle} at each turbine was 'corrected' for the presence of wind shear and turbulence as observed by the SODAR. This correction led to a nacelle 'true-flux' equivalent wind speed ($U_{\text{equivTI\_nacelle}}$, m s^{-1}):

$$U_{\text{equivTI\_nacelle}} = U_{\text{nacelle}} + (U_{\text{equivTI\_SODAR}} - U_{80\_\text{SODAR}}). \quad (11)$$

$U_{\text{equivTI\_nacelle}}$ was calculated for each 10 min period and for each individual turbine.

3. Results

3.1. Climatology and stability

Significant seasonal and diurnal variations in wind speed and power production were present at this wind farm, i.e., wind speeds were higher at night (more power) than during the day (less power) and higher during the warm season (more power) than in the cool season (less power). For all six turbines, average nighttime P_{norm} was 23% in winter, 46% in spring, 67% in summer, and 27% in autumn. Average daytime P_{norm} was 20% in winter, 35% in spring, 43% in summer, and 20% in autumn (figure 1).

This site exhibited stable, near-neutral, and convective stability conditions in a 37:17:44 ratio during the spring and summer. As expected, SODAR stability parameters indicated that daytime hours were almost always strongly convective, convective or near-neutral, while nights were strongly stable, stable, or near-neutral. During very stable conditions, wind shear was significant, positive, and averaged 3.5 m s^{-1} between the bottom and top of the rotor disk. During convective conditions, wind shear was negligible and suggested a well mixed surface layer.

3.2. Estimate of rotor disk wind speed

We compared four measurements of wind speed: (1) nacelle cup anemometer 80 m U, (2) SODAR 80 m U, (3) SODAR 'true-flux' equivalent U, and (4) nacelle-adjusted 'true-flux' equivalent U. Figure 2 shows the frequency distribution of spring and summer wind speeds for each U. The frequency distribution shifted toward lower wind speeds in the nacelle-based measurements as compared to SODAR. This shift likely is due to turbine wake effects on the nacelle cup anemometer (the anemometer is behind the turbine blades) and is most prevalent in the 6–9 m s^{-1} range when all turbulence classes are included (figure 2(a)) but erodes during high turbulence periods (figure 2(c)). Differences between hub-height wind speed and the 'true-flux' rotor-averaged wind speed did not account entirely for the frequency shift between the two instruments. This behavior suggests that the differences in wind speed were instrument-driven or location-driven. Small wind speed differences between hub-height wind speed and 'true-flux' equivalent wind speed are evident in both the nacelle and SODAR data. While these differences are small, they are important for wind power in the region where power generation is related to the wind speed cubed (∼4–12 m s^{-1}). Differences were most acute for wind speeds below 3 m s^{-1} (irrelevant for wind power) and for wind speeds between 8 and 11 m s^{-1}.

To discern the appropriate U for power curves, 10 min power data P_{norm} are plotted as a function of (a) nacelle cup anemometer 80 m U, (b) nacelle cup anemometer 'true-flux' equivalent U, (c) SODAR 80 m U, and (d) SODAR 'true-flux' equivalent U for a typical summer day in figure 3. The uncertainty induced by a non-co-located SODAR wind speed in the power curves can be seen in figures 3(c) and (d). When compared with the manufacturer's power curve, the SODAR-based power curves have lower Pearson's coefficient (r) values (r = 0.88–0.89) than the nacelle-based (r = 0.94–0.95). Furthermore, a small improvement (in terms of a higher r value and lower standard deviation of residuals) is evident from using the nacelle-adjusted 'true-flux' equivalent wind speed instead of the nacelle hub-height U (figure 3(b)). Though small, these differences suggest that the nacelle-adjusted 'true-flux' equivalent wind speed generates the most accurate power curves at this site.

3.3. Stability-stratified power curves

To examine stability-related effects on turbine power performance, 10 min power generation data were segregated into stability classes, based on the wind shear exponent (section 3.3.1), turbulence intensity (section 3.3.2), or turbulence kinetic energy (section 3.3.3) per the categories defined in table 1. Normalized power P_{norm} is plotted as a function of binned nacelle 'true-flux' equivalent wind speed with separate curves for each stability class. Data points are missing in the power curves when there were too few

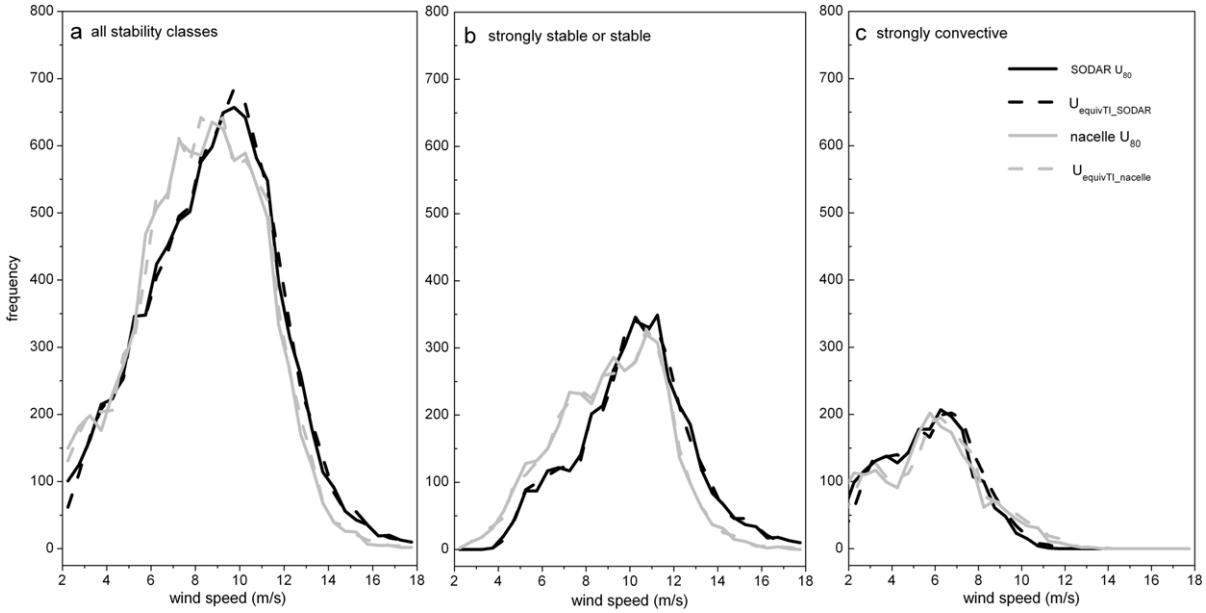

Figure 2. Frequency (# of events) of 10 min SODAR 80 m, SODAR 'true-flux' equivalent, nacelle hub-height, and nacelle-adjusted 'true-flux' equivalent wind speed for Turbine 1 during the spring and summer months. Data are from (a) all stability periods, (b) periods of low turbulence, and (c) periods of high turbulence. The distributions of cup anemometer data are shifted to the left (toward lower wind speeds) during all times except under high turbulence conditions.

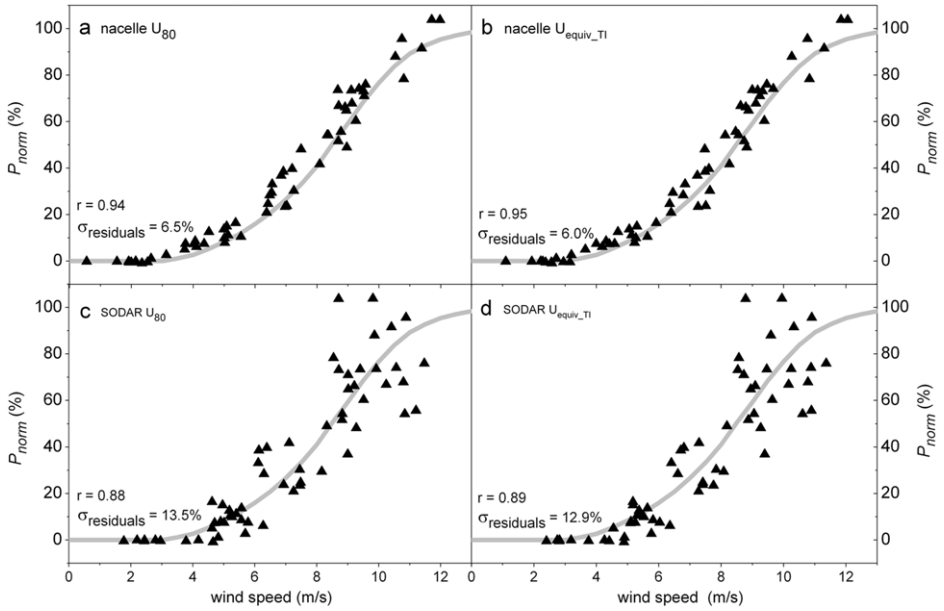

Figure 3. Power curves from a typical summer day based on 10 min normalized power and (a) nacelle hub-height (80 m) wind speed, (b) nacelle-adjusted 'true-flux' equivalent wind speed, (c) SODAR 80 m wind speed, and (d) SODAR 'true-flux' equivalent wind speed. The nacelle and power data are from Turbine 1. Power curve accuracy is based on the 'best fit' metrics (Pearson r value and standard deviation of residuals) between the observations and the manufacturer expected power curve. The plots show that $U_{\text{equivTI\_nacelle}}$ produces the most accurate power curves at this site.

10 min data to statistically represent the 0.5 m s^{-1} wind speed bin. Error bars indicate one standard deviation in power for each velocity bin and stability classification. The power curves shown in all figures are for one turbine, Turbine 1, but are representative of all six turbines examined. Also, the power curves include only strongly stable/stable, convective, or strongly convective regimes to highlight the most distinct power generation differences. Because the warm season is the primary wind power season at this site, the power curves include spring and summer months only.

3.3.1. Wind shear. Using four wind shear parameters (α_{120_40}, α_{120_80}, α_{80_40} and α_{80_50}), 10 min P_{norm} data from Turbine 1 were stratified according to stability regime

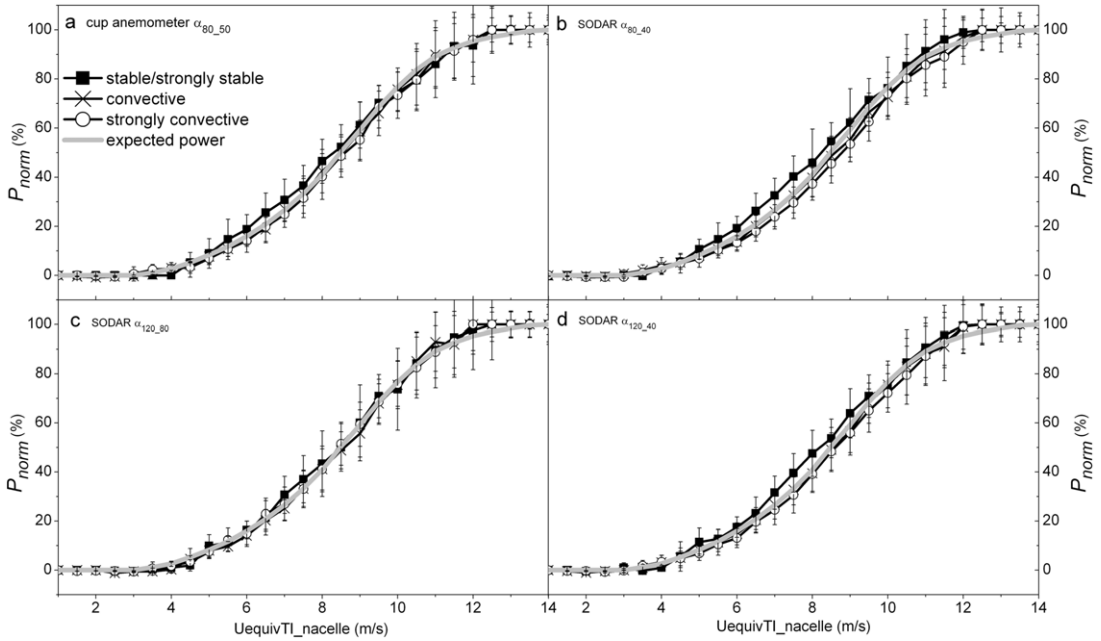

Figure 4. α-stratified power curves for Turbine 1 during strongly convective ($\alpha < 0.0$), convective ($0.0 < \alpha < 0.1$), and stable or strongly stable ($\alpha > 0.2$) atmospheric conditions. Wind shear is based on (a) meteorological tower and (b) SODAR measurements at heights in the lower half of the rotor disk, (c) SODAR measurements at heights in the upper half of the disk, and (d) SODAR measurements at heights across the entire disk. Plotted is mean normalized power ± one standard deviation for each 0.5 m s^{-1} wind velocity bin as well as the manufacturer expected power curve.

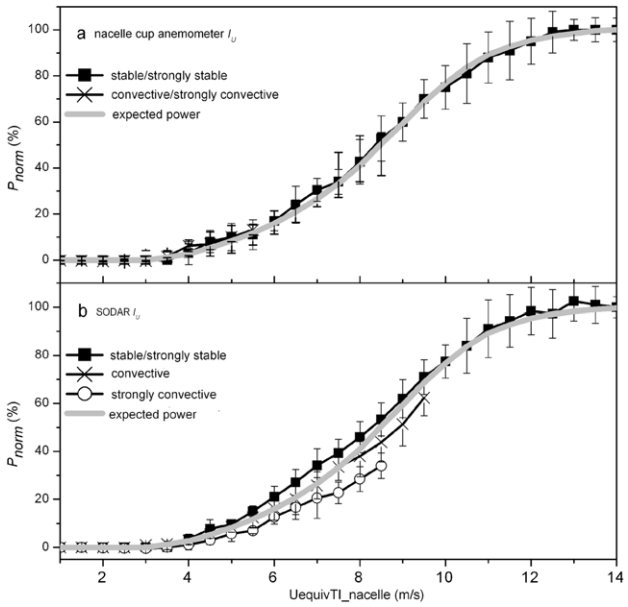

Figure 5. Stability-stratified power curves for Turbine 1 based on (a) nacelle 80 m cup anemometer I_U and (b) 80 m SODAR I_U during strongly stable or stable ($I_U < 10\%$), convective ($I_U > 13\%$, (a)) or ($13\% < I_U < 20\%$, (b)), and strongly convective ($I_U > 20\%$, (b)) conditions, as well as the manufacturer expected power curve. Too few data points were available to plot power observations during strongly convective conditions for the nacelle-based stability (a).

(figure 4). Wind shear in the top half of the rotor disk (α_{120_80}) did not significantly impact power production—the power curves for the three stability classes are nearly indistinguishable (figure 4(c)). However, differences in power production emerge when P_{norm} was stratified by cup anemometer α_{80_50} (figure 4(a)) or SODAR α_{80_40} (figure 4(b)) at heights in the lower half of the rotor disk, or from using wind shear representing the entire disk (α_{120_40}) (figure 4(d)). For example, average P_{norm} during wind speeds of 8 m s^{-1} was 39% ± 5% during strongly convective conditions and 48% ± 4% during stable or strongly stable conditions as compared to an expected P_{norm} of 41% (figure 4(d)). High amounts of wind shear (i.e., stable/strongly conditions) in the lower half or entire rotor disk led to 9% more power produced on average by the turbine as compared to periods of negative shear (i.e., strongly convective conditions) for wind speeds between 6 and 10 m s^{-1}.

3.3.2. Turbulence intensity. The utility of SODAR measurements for understanding power performance is more apparent when considering turbulent intensity. Power curves for Turbine 1 were stratified by nacelle cup anemometer I_U and SODAR I_U in figure 5. Stratification by nacelle I_U (figure 5(a)) included stable or strongly stable periods ($I_U < 10\%$) and convective or strongly convective periods ($I_U > 13\%$). Too few data points were available to isolate the effects of strongly convective conditions for the nacelle-based parameter. Observed power yields followed the expected power curve regardless of stability class. Power differences were less than 5% and occurred when the nacelle 'true-flux' equivalent wind speed was between 4 and 7 m s^{-1}.

In contrast, distinct power curves emerged when the power data were stratified by SODAR measured

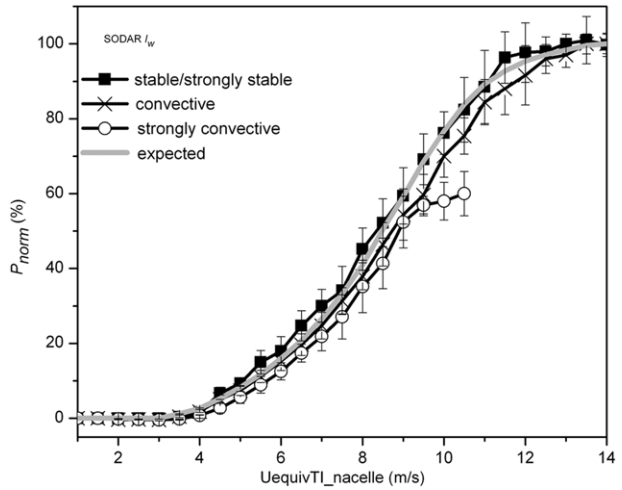

Figure 6. I_w-stratified power curves for Turbine 1 during strongly convective ($I_w > 17\%$), convective ($9\% < I_w < 17\%$), and stable or strongly stable ($I_w < 6\%$) conditions, as well as the expected power curve. Under-performance is observed during strongly convective conditions, especially for higher wind speeds.

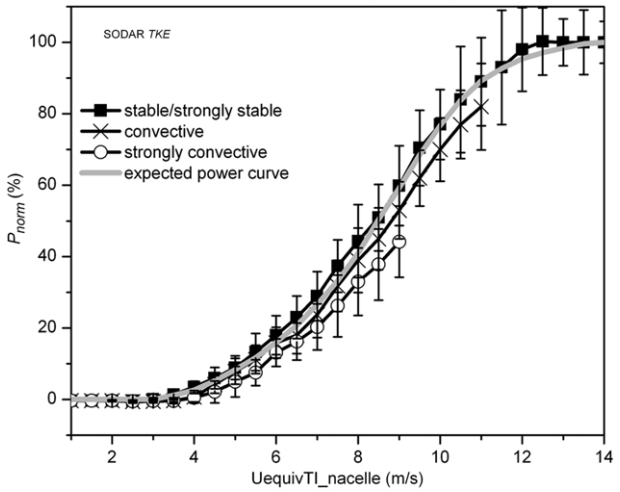

Figure 7. TKE-stratified power curves for Turbine 1 during strongly stable or stable (TKE < 0.7 m^2 s^{-2}), convective (1.0 m^2 s^{-2} $<$ TKE $<$ 1.4 m^2 s^{-2}), and strongly convective conditions (TKE > 1.4 m^2 s^{-2}). Also plotted is the manufacturer expected power curve. Stability-related under-performance is again observed at higher wind speeds for strongly convective conditions.

I_U (figure 5(b)). Figure 5(b) shows power generation data segregated into stable or strongly stable ($I_U <$ 10%), convective (13% $I_U <$ 20%), or strongly convective ($I_U > 20\%$) conditions. The most significant power curve differences occurred between very stable/stable and very convective conditions for wind speeds 7.0–8.5 m s^{-1}. In general, Turbine 1 over-performed during stable/strongly stable conditions for 5.5–8 m s^{-1} wind speeds and under-performed during strongly convective conditions for all wind speeds above 5.5 m s^{-1}. Greatest under-performance occurred at moderate wind speeds (7.0–8.5 m s^{-1}) during strongly convective conditions. For example, for a wind speed of 7.5 m s^{-1}, mean P_{norm} was 40% $\pm$ 6% during strongly stable/stable conditions and 23% $\pm$ 4% during strongly convective conditions, compared to the expected P_{norm} of 33%. Among all six turbines examined, differences in normalized power between stable/strongly stable (more power) and strongly convective (less power) conditions ranged from 10 to 20%.

Extraneous noise (e.g., spikes in the measurements) may occur in the SODAR horizontal velocity data and could exaggerate power distinctions. To remove this possible bias in the I_U power curves, power data were stratified by vertical turbulence intensity I_w. Power data were binned into stable or strongly stable conditions ($I_w < 6\%$), convective conditions ($9\% < I_w <$ 17%), or strongly convective conditions ($I_w >$ 17%) (figure 6). Power deficiencies were observed for every wind speed above turbine cut-in speed ($U > 3.5$ m s^{-1}) during strongly convective conditions. Under-performance was particularly high for winds between 10.5 and 11 m s^{-1}; Turbine 1 produced just 75% of expected power. Over-performance was less evident during stable/strongly stable conditions and reached +3% in the 5–8 m s^{-1} wind speed range.

3.3.3. Turbulence kinetic energy. Distinct power differences also emerged when P_{norm} was stratified by turbulence kinetic energy (TKE). The most significant power deviations occurred during strongly convective conditions (TKE $>$ 1.4 m^2 s^{-2}); these differences approached 18% between expected power and the amount of power produced (figure 7). For example, at 9 m s^{-1}, average P_{norm} was 44% $\pm$ 10% during strongly convective conditions, as compared to an expected P_{norm} of 60%. During stable/strongly stable conditions (TKE $<$ 0.7 m^2 s^{-2}), over-performance was smaller than observed with either SODAR-based I_U (figure 5(b)) or α (figure 4(d)) and approached +5%.

4. Discussion

Data from a well-instrumented wind farm enabled assessment of atmospheric stability impacts on power generation. This study builds on stability-related, rotor disk wind speed trends presented in Wharton and Lundquist (2012) for a megawatt wind farm. Other wind power studies have determined atmospheric stability based on one or two stability parameters, e.g., Motta *et al* (2005) and van den Berg (2008), while ours is the first study to our knowledge that relates power production to a large set of independent stability parameters, including SODAR-derived I_w and TKE. Previous studies into the influence of stability on wind power have not found universal agreement (e.g., Hunter *et al* 2001, Antoniou *et al* 2009). In our study, we found that high wind shear ($\alpha > 0.2$) had a positive effect on power production for the 5–10 m s^{-1} range, while negative wind shear had a negative impact on power except for wind speeds above 12 m s^{-1}. For low-to-moderate wind speeds (<5 m s^{-1}), we observed that wind shear had little impact on power performance. For the 5–8.5 m s^{-1} wind range, we found that very high amounts of turbulence decreased power production by an average of 15%. This result contradicts observations made by Elliott and Cadogan (1990) who found that higher turbulence led

to more power for wind speeds between 4 and 8 m s^{-1}. However, their site experienced different stability-related meteorological conditions than the one examined here. In their study, the rotor-averaged wind speed was less than hub-height wind speed under stable conditions. Therefore, less energy was available to turbines during stable conditions than during convective. In contrast, we found a higher rotor-averaged wind speed than hub-height wind speed under stable conditions and, consequently, greater energy production. We observed a negative impact of turbulence on power production: power decreased as the boundary layer became more convective, coinciding with a lower 'true-flux' equivalent wind speed, higher turbulence, and small or negative wind shear across the rotor disk. It is important to note that our location experiences strong, channeled flow in the spring and summer months. Therefore, our stable conditions did not experience the strong veering of the wind vector with height (i.e., directional shear) as is common at locations with nocturnal low-level jets (e.g., Banta *et al* 2002). Strong directional shear can undermine the performance of a turbine, which might explain why some studies find under-performance during stable conditions at high wind speeds (Rareshide *et al* 2009). At our location, however, we consistently and repeatedly observed under-performance during strongly convective conditions.

It is important to consider that atmospheric turbulence and wind shear are intrinsically related, e.g., turbulence erodes to shear and shear leads to turbulence. As such, the exact effects of turbulence on power generation versus wind shear on generation are hard to distinguish. A low turbulence intensity parameter generally includes conditions with high wind shear and vice versa, while a low wind shear parameter usually occurs during times of high turbulence. To distinguish the individual effects of turbulence versus wind shear on power production, very high time resolution (>10 Hz) turbulence measurements are needed so that the coherent structures of turbulence can be properly identified. Unfortunately, such data were not available to us at this wind farm but this topic warrants further investigation for other sites.

Based on our findings, we offer these recommendations.

4.1. Accurate power curves require a 'true-flux' equivalent wind speed

Due to variability in wind shear and turbulence, a significant source of error or uncertainty in power curves will be generated by differences between the true disk-averaged velocity and hub-height velocity. These errors may appear in modeling studies as well, and simulations, such as Wang and Prinn (2011) reported, must account for variations of atmospheric stability when considering power performance of turbines.

4.2. Nacelle-based measurements do not lend insight into power differences

Nacelle-based turbulence intensity did not enable useful distinctions of stability regimes to isolate influences on power production. This finding is supported by the weak correlation between nacelle I_U and the Obukhov length stability parameter (Wharton and Lundquist 2012) and studies by Hölling *et al* (2007), Finnigan (2002), and Kline (2008) which show that cup anemometers are unable to measure high turbulence even in controlled wind tunnels. Instruments with higher accuracy and sampling frequency are needed in wind power studies.

5. Conclusions

This work highlights the benefit of observing nearly complete profiles of wind speed and turbulence across the turbine rotor disk. Here, the presence of a nighttime, stable boundary layer, with little or no directional shear, had the same effect on power performance as increasing the wind velocity at hub-height by 0.2 m s^{-1}. The opposite was true for strongly convective conditions. Very high turbulence and low shear had the same effect on power as decreasing hub-height wind speed by 0.5–1.0 m s^{-1}. These results suggest that wind energy resource assessment and short-term (day ahead) power forecasting would likely benefit from increased accuracy if atmospheric stability impacts are measured and appropriately incorporated in power forecasts, such as through generation of power curves based on a range of turbulence regimes.

Acknowledgments

The authors express appreciation to Iberdrola Renewables, Inc. for sharing their wind farm data. We also acknowledge helpful suggestions by Neil Kelley and Dennis Elliott of NREL. This work was funded by the Department of Energy's Wind and Water Power Program Office under the Renewable Systems Interconnect Support Program (BNR-EB2502010) and performed under the auspices of the US Department of Energy by Lawrence Livermore National Laboratory under Contract DE-AC52-07NA27344. LLNL is operated by Lawrence Livermore National Security, LLC, for the DOE, National Nuclear Security Administration under Contract DE-AC52-07NA27344. NREL is a national laboratory of the US Department of Energy, Office of Energy Efficiency and Renewable Energy, operated by the Alliance for Sustainable Energy, LLC.

References

Antoniou I, Jørgensen H E, Ormel F, Bradley S, von Hünerbein S, Emeis S and Warmbier G 2003 *On The Theory of SODAR Measurement Techniques* (Roskilde: Risø National Laboratory) p 59

Antoniou I, Pedersen S M and Enevoldsen P D 2009 Wind shear and uncertainties in power curve measurement and wind resources *Wind Eng.* **33** 449–68

Antoniou I, Wagner R, Pedersen S M, Paulsen U, Madsen H A, Jørgensen H E, Thomsen K, Enevoldsen P and Thesbjerg L 2007 Influence of wind characteristics on turbine performance *Proc. European Wind Energy Conference and Exhibition (Milan)*

Banta R M, Newsom R K, Lundquist J K, Pichugina Y L, Coulter R L and Mahrt L 2002 Nocturnal low-level jet characteristics over Kansas during CASES-99 *Bound.-Layer Meteorol.* **105** 221–52

Betz A 1966 *Introduction to The Theory of Flow Mechanics* (Oxford: Pergamon) p 281

Christensen C J and Dragt J B (ed) 1986 Accuracy of power-curve measurements *Risø-M-2632* (Roskilde: Risø National Laboratory)

Elliott D L and Cadogan J B 1990 Effects of wind shear and turbulence on wind turbine power curves *Proc. European Community Wind Energy Conference and Exhibition (Madrid)*

Elliott D L, Holliday C, Barchet W, Foote H and Sandusky W 1987 *Wind Energy Resource Atlas of the United States* (Golden, CO: Solar Energy Research Institute, DOE/CH 10093-4) p 210

Finnigan J J 2002 Instrumentation II: vector wind sensors *Advanced Short Course on Agricultural, Forest and Micro Meteorology* ed F Rossi, P Duce and D Spano (Sassari: Consiglio Nazionale Delle Ricerche) pp 160–71

Fransden S 1987 On uncertainties in power performance measurements *Proc. 6th ASME Wind Energy Symp.* (New York: American Society of Mechanical Engineers)

Gaynor J E and Kristensen L 1986 Errors in second moments estimated from monostatic Doppler Sodar winds, part II: application to field measurements *J. Atmos. Ocean. Technol.* **3** 529–34

Gottschall J and Peinke J 2008 How to improve the estimation of power curves for wind turbines *Environ. Res. Lett.* **3** 015005

Hölling M, Schulte B, Barth S and Peinke J 2007 Sphere anemometer—a faster alternative solution to cup anemometry, The science of making torque from wind *J. Phys.: Conf. Ser.* **75** 012064

Honhoff S 2007 Power curves—the effect of environmental conditions *Proc. GE Wind AWEA Wind Speed and Energy Workshop (Portland, OR)*

Hunter R, Pedersen T F, Dunbabin P, Antoniou A, Frandsen S, Klug H, Albers A and Lee W K 2001 *European Wind Turbines Testing Procedure Developments. Task 1: Measurement Method to Verify Wind Turbine Performance Characteristics RISOE R-1209* (Roskilde: Risø National Laboratory)

IEC (International Electromechanical Commission) 2003 Wind turbines—Part 12-1: Power performance measurements of electricity producing wind turbines *Technical Report No. IEC 61400-12-1* (Geneva: IEC)

Ito Y 1997 Errors in wind measurements estimated by five-beam array Doppler Sodar *J. Atmos. Ocean. Technol.* **14** 792–801

Kaiser K, Hohlen H and Langreder W 2003 Turbulence correction for power curves *Proc. European Wind Energy Conference and Exhibition (Madrid)*

Kline J 2008 Addressing bias in wind measurements: part 1 *Proc. AWEA Wind Resource and Project Energy Assessment Workshop (Portland, OR)*

Mann J, Sorensen J N and Morthorst P-E 2008 Wind energy *Environ. Res. Lett.* **3** 015001

Motta M, Barthelmie R J and Vølund P 2005 The influence of non-logarithmic wind speed profiles on potential power output at Danish offshore sites *Wind Energy* **8** 219–36

Rareshide E, Tindal A, Johnson C, Graves A M, Simpson E, Bleeg J, Harris T and Schoborg D 2009 Effects of complex wind regimes on turbine performance *Proc. American Wind Energy Association WINDPOWER Conference (Chicago, IL)*

Rohatgi J and Barbezier G 1999 Wind turbulence and atmospheric stability—their effects on wind turbine output *Renew. Energy* **16** 908–11

Sumner J and Masson C 2006 Influence of atmospheric stability on wind turbine power performance curves *J. Sol. Energy Eng.* **128** 531–7

Tindal A, Johnson C, LeBlanc M, Harman K, Rareshide E and Graves A-M 2008 Site-specific adjustments to wind turbine power curves *Proc. American Wind Energy Association WINDPOWER Conference (Houston, TX)*

van den Berg G P 2008 Wind turbine power and sound in relation to atmospheric stability *Wind Energy* **11** 151–69

Wagner R, Antoniou I, Pedersen S M, Courtney M S and Jørgensen H E 2009 The influence of the wind speed profile on wind turbine performance measurements *Wind Energy* **12** 348–62

Wang C and Prinn R G 2011 Potential climatic impacts and reliability of large-scale offshore wind farms *Environ. Res. Lett.* **6** 025101

Wharton S and Lundquist J K 2012 Assessing atmospheric stability and its impacts on rotor-disk wind characteristics at an onshore wind farm *Wind Energy* at press (doi:10.1002/we.483)